RSC Advances

PAPER

View Article Online
View Journal | View Issue

Cite this: *RSC Adv.*, 2019, **9**, 12124

Enhanced electrocatalytic hydrodechlorination of 2,4-dichlorophenoxyacetic acid by a Pd-Co_3O_4/Ni foam electrode

Qiuxiang Liu,[ab] Yanting Shen,[b] Shuang Song [ab] and Zhiqiao He *[b]

Received 11th March 2019
Accepted 9th April 2019

DOI: 10.1039/c9ra01843c

rsc.li/rsc-advances

A new Pd-Co_3O_4/Ni foam electrode was synthesized by a facile two-step method comprising co-electrodeposition and calcination. Compared with Ni foam-supported Pd electrodes obtained by electrodeposition or chemical deposition, the new Pd-Co_3O_4/Ni foam electrode exhibited greatly enhanced catalytic hydrodechlorination activity. The introduction of Co_3O_4 reduced the amount of Pd required. For the same degree of dechlorination of 2,4-D, only 25% of the Pd was required in the Pd-Co_3O_4/Ni foam electrode compared with the Ni foam electrode prepared by chemical deposition. Various characterizations indicated that Co_3O_4 on the surface of the Ni foam enhanced catalytic performance through accelerated generation of atomic H*. In addition, the good distribution of macropores, providing a larger specific surface area and lower electron transfer impedance, enabled more adsorption of atomic H^*_{ads}.

1. Introduction

The chlorinated organic compound (COC) 2,4-dichlorophenoxyacetic acid (2,4-D) is a commonly used herbicide to control a wide range of broadleaf weeds and grasses in crops because of its low cost and good selectivity.[1,2] However, 2,4-D is a weakly biodegradable pollutant that is easily transported into bodies of water as a result of leaching and surface runoff.[3–5] Additionally, studies on the toxicological effects of 2,4-D have shown that it is a threat to public health.[6,7] Some studies have reported toxicity of 2,4-D as a consequence of endocrine disrupting activities in animals and humans, causing irreparable damage to the central nervous system. The prevalence and toxicity of 2,4-D have prompted research into the reductive dechlorination of COCs to form less dangerous products.[8–11]

Compared with various methods of reduction, including chemical and biological methods and photochemical dechlorination,[12–15] electrocatalytic reductive dechlorination is considered to be efficient because of intrinsic advantages such as mild reaction conditions, rapid reaction rate and the absence of recalcitrant secondary contaminants.[9,16–18] The electrolytic dechlorination of COCs has been studied on Ag, Au, Pd, Pt, Cu, Fe, Ni, Pb, Zn.[19] In particular, palladium (Pd) is generally utilized as the catalyst for hydrodechlorination reactions.[20,21] The metal has the ability to retain large amounts of nascent adsorbed atomic H^*_{ads} *via* Pd–H bonds that result from multiple σ-bonding interactions between hydrogen atoms and the d orbitals of the Pd atoms.[22,23] However, Pd is expensive and it is desirable to make the electrocatalytic hydrodechlorination process more economically feasible. Transition metal oxides and some low cost metals, such as TiO_2, CeO_2, NiO, Co_3O_4, Cu and Ag,[24–28] have shown potential as co-catalysts to reduce the amount of precious metal catalyst, increase catalytic activity, enhance tolerance to catalyst poisoning, and they cost less than precious metals.

Recently, there has been widespread application of transition metal oxides (Fe_3O_4, Co_3O_4 and NiO) for hydrogen production *via* the hydrogen evolution reaction (HER) as water-splitting electrocatalysts in the field of energy research.[29–32] According to the well-known theoretical "Volcano Curve",[33] the catalytic performance of Co is slightly inferior to those of the expensive platinum group metals such as Pt, Pd and Ir. It has been demonstrated by other researchers that Co_3O_4 enhances the performance of HER.[34] Since H_2 molecules would readily dissociate on the surface of Pd,[35] it is expected that Co_3O_4 could be used to improve the activity of Pd in electrochemical hydrodechlorination of 2,4-D.

In this work, hybrids of Pd and Co_3O_4 supported on Ni foam (Pd-Co_3O_4/Ni foam) were fabricated by co-electrodeposition followed by calcination, and used as electrodes for electrochemical hydrodechlorination of 2,4-D. Ni foam was selected as the electrode substrate because of its large specific surface area, porous structure and excellent electrical conductivity.[36–38] The reaction mechanism and pathway of 2,4-D dechlorination by the Pd-Co_3O_4/Ni foam electrode were also studied.

[a]*Collaborative Innovation Center of Yangtze River Delta Region Green Pharmaceuticals, Zhejiang University of Technology, Hangzhou 310032, People's Republic of China*

[b]*College of Environment, Zhejiang University of Technology, Hangzhou 310032, People's Republic of China. E-mail: zqhe@zjut.edu.cn; Fax: +86-571-88320276; Tel: +86-571-88320726*

2. Experimental

2.1. Materials

All chemical reagents used in this study were of analytical grade and purchased from Huadong Medical Co., Ltd, China. Nickel foam with a pore density of 110 ppi was purchased from Suzhou Jiashide Materials, Ltd, China. Ultra-pure water (18.2 mΩ cm^{-1}) was obtained from a Millipore-Q system.

2.2. Electrode preparation

In a typical procedure, a piece of Ni foam (20 × 20 × 1.2 mm) was used as the substrate for electrodeposition. Before electrode preparation, the Ni foam was dipped in acetone in an ultrasonic bath for 20 min, rinsed with H_2SO_4 solution (0.5 mol L^{-1}) for 5 min to remove the surface oxidized layer,[39] and then rinsed with ultrapure water and dried in a stream of nitrogen. The electrodeposition device was a standard three-electrode glass cell (100 mL) consisting of the clean Ni foam working electrode, a platinum plate counter electrode and a saturated calomel electrode (SCE) in a water bath (THD-2015, Ningbo Tian Heng Instrument Factory, China) at 25 °C ± 1 °C. All of the potentials mentioned in this paper are relative to the SCE unless otherwise specified. Firstly, the Ni foam was subjected to constant potential deposition at −1.0 V for 20 min in a 40 mL aqueous solution containing 5 mmol L^{-1} $Co(NO_3)_2$ and 1 mmol L^{-1} $PdCl_2$. The treated Ni foam electrode was carefully rinsed several times with ultrapure water and dried in N_2. Subsequently, the electrode was placed in a quartz tube and calcined at 250 °C for 120 min with a ramping rate of 1 °C min^{-1} to transform into the hybrid Pd-Co_3O_4/Ni foam electrode. The Pd loading was determined to be 0.47 mg cm^{-2} using inductively coupled plasma optical emission spectrometry (ICP-OES) by dissolution of the electrode in nitrohydrochloric acid. Two other electrodes with the same Pd loading (0.47 mg cm^{-2}) were prepared for comparison: constant potential deposition of Pd on Ni foam (Pd(CPD)/Ni foam) was performed at −1.0 V for 25 min in a 40 mL aqueous solution containing 1 mmol L^{-1} $PdCl_2$; chemical deposition of Pd on Ni foam (Pd(CD)/Ni foam) was carried out according to a published method.[40] In addition, the Pd(CD)/Ni foam electrode was prepared with 4 times the Pd loading (4Pd(CD)/Ni foam). The Co_3O_4 supported on the Ni foam (Co_3O_4/Ni foam) electrode was prepared using the same method used for Pd-Co_3O_4/Ni foam in the absence of $PdCl_2$.

2.3. Batch experiments

Electrochemical dechlorination of 2,4-D was conducted in a conventional two-compartment glass H-cell in a water bath at 25 °C ± 1 °C. The initial concentration of 2,4-D (50 mg L^{-1}) was selected to be within the usual range for chlorinated organic compounds found in agricultural wastewater.[41] The cathode (80 mL) and anode (50 mL) compartments were separated by Nafion-117 membranes, and the catholyte was magnetically stirred during electrolysis. In each experiment, aqueous Na_2SO_4 solution (0.017 mol L^{-1}, 30 mL) containing 2,4-D (50 mg L^{-1}) was added into the cathode compartment and aqueous Na_2SO_4 (0.017 mol L^{-1}, 25 mL) was added into the anode compartment. The cathode (modified Ni foam) and anode (platinum foil) were placed vertically at a separation of about 80 mm. The surface of the working electrode exposed to electrolytes was a square film with a geometric surface area of 4 cm^2. Platinum foil with a surface area of 4 cm^2 was used as the counter electrode and a SCE was used as the reference electrode. A constant current of 0.006 A was supplied by the electrochemical workstation (CHI760E Shanghai Chen Hua Instrument Co., China) for 120 min. Samples (0.4 mL) were withdrawn from the catholyte at predetermined time intervals for analysis.

The concentrations of 2,4-D, 2-chlorophenoxyacetic acid (2-CPA), 4-chlorophenoxyacetic acid (4-CPA) and phenoxyacetic acid (PA), were analyzed on an Agilent 1200 series high-performance liquid chromatograph (HPLC) equipped with an Agilent XDB-C18 column (150 × 4.6 mm). The mobile phase was methanol/water (0.2% H_3PO_4) (60/40 by volume) at a flow rate of 0.8 mL min^{-1}. The chosen determination wavelength was 210 nm and the volume of the injected sample was 5 μL.

The current efficiency (CE) for the 2,4-D dechlorination was calculated using eqn (1):

$$\mathrm{CE} = \frac{(n_1 C_{\mathrm{PA}} + n_2(C_{2-\mathrm{CPA}} + C_{4-\mathrm{CPA}}))FV}{\int_{t=0}^{t=t} I\mathrm{d}t} \quad (1)$$

where n_1 and n_2 represent the electron transfer numbers for the generation of one molecule of PA ($n_1 = 4$) and CPA ($n_2 = 2$), respectively; C_{PA}, $C_{2\text{-CPA}}$ and $C_{4\text{-CPA}}$ denote the concentrations, at electrolysis time t, of PA, 2-CPA and 4-CPA, respectively; F is the Faraday constant, V is the volume of the total catholyte, and I is the electrolysis current.

2.4. Electrode characterization

The Pd loading on the electrodes was analyzed by ICP-OES (Optima 7000DV, PerkinElmer Co. Ltd, USA). The morphology of the electrodes was analyzed by scanning electron microscopy (SEM, ΣIGMA, Carl Zeiss, Germany) coupled with energy dispersive X-ray spectroscopy (EDS, XFlash Detector 5010, Bruker Optics, Germany) operating at an accelerating voltage of 5 kV. The X-ray diffraction (XRD, D/max 2550/PC, Rigaku, Japan) patterns were recorded using Cu Kα radiation (λ = 1.5418 Å), operated at 40 kV and 30 mA and a scan rate of 10° min^{-1}. X-ray photoelectron spectroscopy (XPS, 5000C ECSA system, PHI Co., USA) was conducted using a Mg-Kα source ($h\nu$ = 1253.6 eV). The Brunauer–Emmett–Teller (BET) method was used to determine the surface area of the electrodes (ASAP 2020, McMeretik Instruments Co., Ltd, China).

To study the electrocatalytic activity of Pd-Co_3O_4/Ni foam, linear sweep voltammetry (LSV), cyclic voltammetry (CV) and electrochemical impedance spectroscopy (EIS) analyses were performed on the prepared electrodes (20 × 20 × 1.2 mm) in a conventional three-electrode system using an electrochemical workstation. Platinum foil and SCE were used as the counter electrode and reference electrode, respectively. The electrolyte was 0.1 mol L^{-1} aqueous Na_2SO_4, which was purged with high purity N_2 for 10 min to remove dissolved O_2. The LSV curves were determined from −1.5 to 0 V at 20 mV s^{-1} and CV scans were recorded between −1.0 and 0.0 V at 50 mV s^{-1}. The EIS spectra

were recorded over the frequency range of 0.1–1000 kHz with a 5 mV amplitude at an open circuit voltage. For comparison, the electrocatalytic activities of Ni, Co_3O_4/Ni, and Pd(CPD)/Ni foam samples were measured under similar conditions.

3. Results and discussion

3.1. Characterization

Fig. 1 shows the XRD patterns of Pd-Co_3O_4/Ni, Pd(CPD)/Ni and Pd(CD)/Ni foams. As can be seen, diffraction peaks assigned to (111), (200) and (220) planes of Ni (JCPDS card no. 04-0850),[42] and the (111) plane of Pd (JCPDS card no. 46-1043)[43] were observed on all three electrodes. One differing feature was the presence of three weak typical diffraction peaks at 36.8°, 59.3° and 65.2° corresponding to the (311), (511), and (440) planes of Co_3O_4 (JCPDS card no. 042-1467)[44] on the Pd-Co_3O_4/Ni foam. This confirmed that Co_3O_4 and Pd were successfully deposited onto the surface of the Ni foam.

XPS was used to characterize the elemental composition and understand the chemical states of Pd and Co on the surface of the Ni foam electrode. The overall XPS spectrum (Fig. 2(a)) of the Pd-Co_3O_4/Ni foam exhibited peaks corresponding to Co 2p, O 1s, Pd 3d and C 1s. High resolution XPS spectra of Co 2p, Pd 3d and O 1s are shown in Fig. 2(b–d). The high resolution XPS spectrum of Co 2p showed two peaks at binding energies of 779.8 and 794.8 eV with a spin-energy separation of 15 eV. These two peaks are ascribed to Co $2p_{3/2}$ and Co $2p_{1/2}$, respectively, which is in good agreement with reports in the literature on the characterization of Co_3O_4.[45,46] The Pd 3d spectrum contained two spin–orbit peaks that corresponded to signals for Pd $3d_{5/2}$ and Pd $3d_{3/2}$ at binding energies of 336.6 and 342.0 eV, respectively. The value of 336.6 eV was higher than the binding energy for metallic Pd $3d_{5/2}$ (335.4 eV) due to superficial oxidation of Pd as a consequence of the nano-scale nature of the Co_3O_4 and Pd co-deposition on the Ni foam.[47,48] The high resolution XPS spectrum of O 1s was fitted into two peaks at binding energies of 529.8 and 530.8 eV, corresponding to the Co–O bond and surface absorbed water, respectively.[49–51]

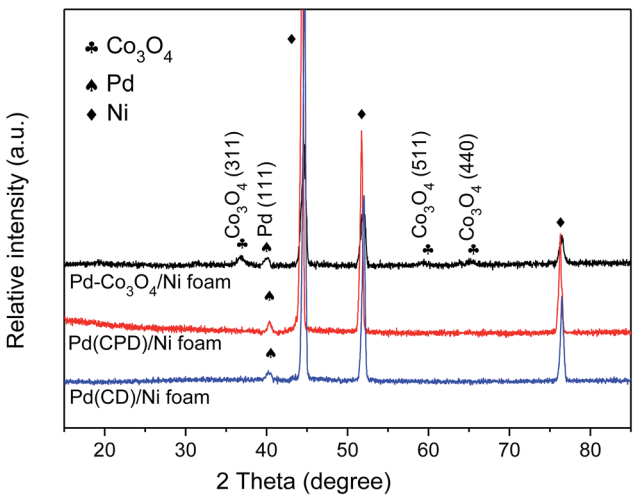

Fig. 1 The XRD patterns of Pd-Co_3O_4/Ni, Pd(CPD)/Ni and Pd(CD)/Ni foams.

Fig. 3 shows the determination of elemental composition of the electrode surface by EDS analysis. As can be seen, Ni, Co, O and Pd were present on the Pd-Co_3O_4/Ni foam, while only Ni, Pd and a small amount of oxygen, caused by surface oxidation of the metals, were present on the Pd(CD)/Ni and Pd(CPD)/Ni foam electrodes.

The XRD and XPS characterizations confirmed the presence of Pd and Co_3O_4 on the surface of the Ni foam after constant potential deposition at a potential of −1.0 V and calcining at 250 °C. The EDS spectrum further confirmed the result.

The preparation of the Pd-Co_3O_4/Ni foam electrode was achieved in two steps. In the first step, a green $Co(OH)_2$ precursor and Pd were co-electrodeposited onto the Ni foam at a potential of −1.0 V. The origin of $Co(OH)_2$ generation has been explained previously.[37] Electrodeposition of Pd on the Ni foam surface at a potential of −1.0 V has also been reported in the literature.[52] In the second step, $Co(OH)_2$ was calcined in air at 250 °C and transformed to black Co_3O_4 in a simple oxidation reaction. ICP-OES results showed a Pd loading of 0.47 mg cm^{-2} and a cobalt loading of 0.4 mg cm^{-2}.

Fig. 4 shows the surface morphological properties of the fresh Ni foam, as-prepared Pd(CD)/Ni foam, Pd(CPD)/Ni foam and Pd-Co_3O_4/Ni foam electrodes. As observed in Fig. 4(a), the fresh Ni foam exhibited an irregular block structure with grooves on the surface. An irregular dense agglomeration of Pd particles was formed on the Pd(CD)/Ni foam electrode after chemical deposition (Fig. 4(b)), which was warped in many places because of weak contact with the Ni foam substrate. In contrast, Fig. 4(c) shows that the Pd particles were more uniformly dispersed on the surface of Pd(CPD)/Ni and tightly bound to the Ni foam. Comparison of Fig. 4(c) and (d) reveals that Pd particles and Co_3O_4 nanosheets were evenly deposited on the surface of the Pd-Co_3O_4/Ni foam electrode. The Co_3O_4 nanosheets lay aslant or perpendicular, were evenly deposited on the surface of the Ni foam and interconnected with Pd particles, providing a highly open and porous structure. The open porous channels between the Co_3O_4 nanosheets and Pd particles facilitated fast penetration of the electrode.[37] In other words, these hierarchical multi-porous structures ensured efficient contact between surface active sites and the electrolyte.[53,54] Furthermore, the ultrathin macroporous surface facilitated electron transfer across the electrode surface. Therefore, the introduction of Co_3O_4 provided a particular surface morphology that the Pd(CD)/Ni and Pd(CPD)/Ni foams cannot.

According to the results of the BET test, the surface areas of the Pd(CD)/Ni, Pd(CPD)/Ni and Pd-Co_3O_4/Ni foam electrodes were 3.7, 4.3 and 8.5 m^2 g^{-1}, respectively, which also demonstrated that the Pd and Co_3O_4 co-deposition electrodes had larger surface areas. The larger surface area of the electrode provided more active sites for dechlorination reaction.

3.2. Comparative experiments with different electrodes

In general, the current density is a significant factor affecting the removal rate of 2,4-D by catalytic electrodes. As shown in Fig. 5(f), an increase of the applied current density from 0.5 to 1.5 mA cm^{-2} resulted in increased removal efficiency of 2,4-D

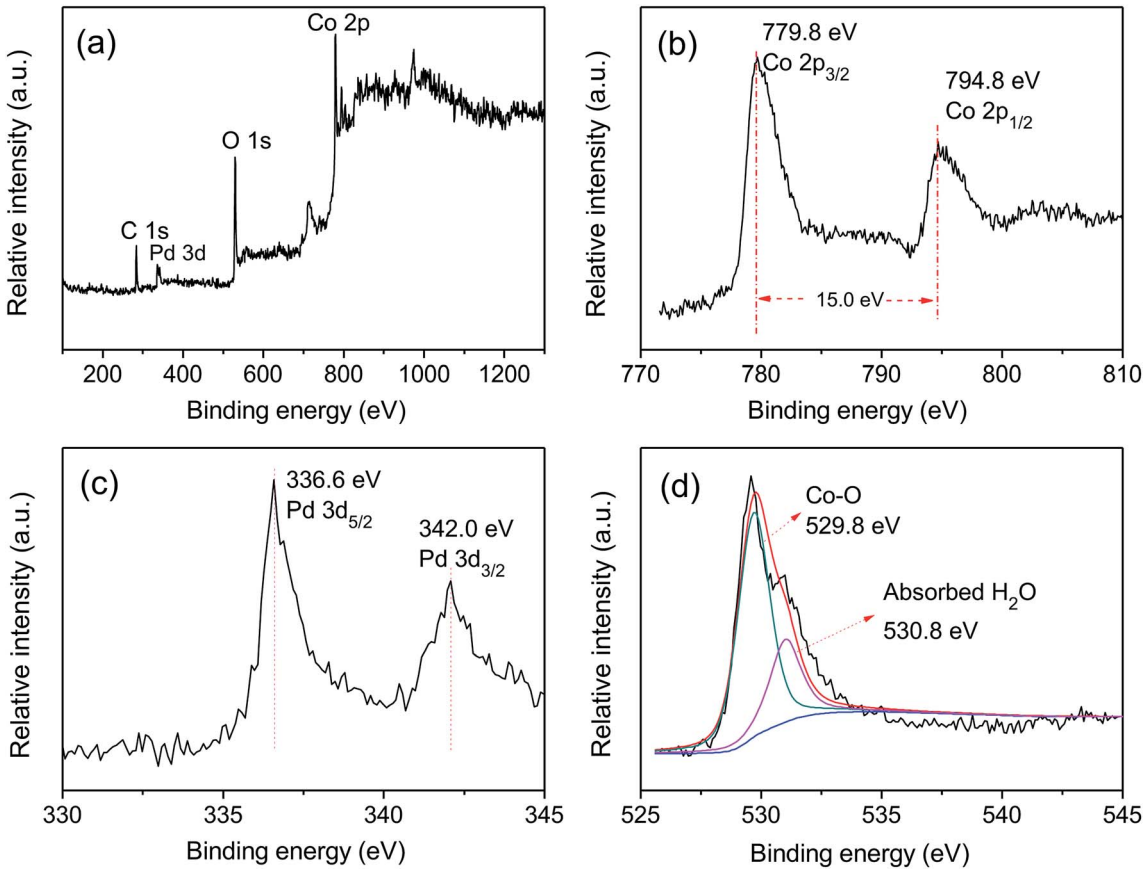

Fig. 2 The XPS spectra of (a) overall spectra, (b) Co 2p, (c) Pd 3d and (d) O 1s for the Pd-Co_3O_4/Ni foam.

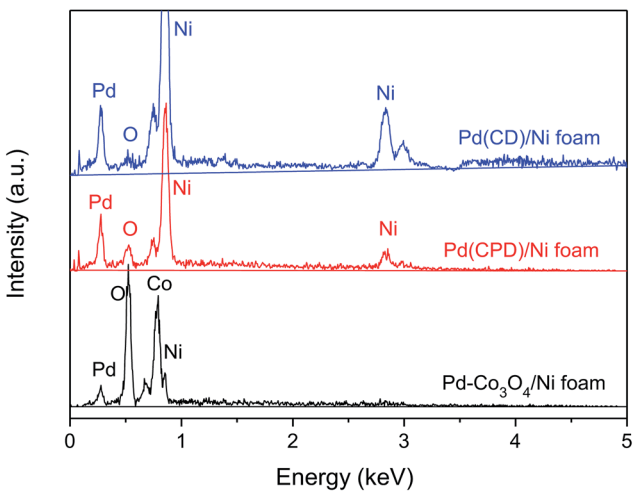

Fig. 3 The EDS spectra of Pd-Co_3O_4/Ni, Pd(CPD)/Ni and Pd(CD)/Ni foams.

from 22.5% to 94.2% during 60 min electrolysis. A further increase of current density to 2.5 mA cm^{-2} led to a slight reduction of dechlorination efficiency. This is because the high current density provides sufficient H^*_{ads} for the electrocatalytic hydrodechlorination, but an excessive current density accelerates H_2 generation, retarding mass transfer of the chlorinated organic material to the reaction active site. Thus, the optimal current density for removal of 2,4-D is 1.5 mA cm^{-2}.

To compare electrocatalytic activity, removal of 2,4-D by electrochemical hydrodechlorination was conducted with as-prepared Ni, Co_3O_4/Ni, Pd(CD)/Ni, Pd(CPD)/Ni, 4Pd(CD)/Ni and Pd-Co_3O_4/Ni foams. Fig. 5(a) shows the time course for reaction of 2,4-D. After 120 min of electrolysis, hardly any 2,4-D was removed by the bare Ni foam, while 67.2% and 61.5% were removed by the Pd(CPD)/Ni foam and Pd(CD)/Ni foam, respectively. This was because Pd is a well-known catalyst that promotes dechlorination.[55,56] The dechlorination of 2,4-D was remarkably enhanced by the Pd-Co_3O_4/Ni foam, and 94.2% of 2,4-D was removed after 60 min, indicating that the presence of Co_3O_4 played an important role in dechlorination. However, the rate of removal of 2,4-D by the Co_3O_4/Ni foam in the absence of Pd was similar to that using the bare Ni foam, which implied that Co_3O_4 acted as a co-catalyst for dechlorination. It is worthwhile noting that four times the amount of Pd (1.88 mg cm^{-2}) in the 4Pd(CD)/Ni foam was required to achieve similar removal efficiency to the Pd-Co_3O_4/Ni foam (Fig. 5(a)). The results demonstrated that the Pd-Co_3O_4/Ni foam electrode significantly reduced the amount of Pd required while maintaining good dechlorination performance.

The molar concentrations of intermediates and the final product as a function of time for various electrodes at a current density of 1.5 mA cm^{-2} are shown in Fig. 5(a–d). As can be seen

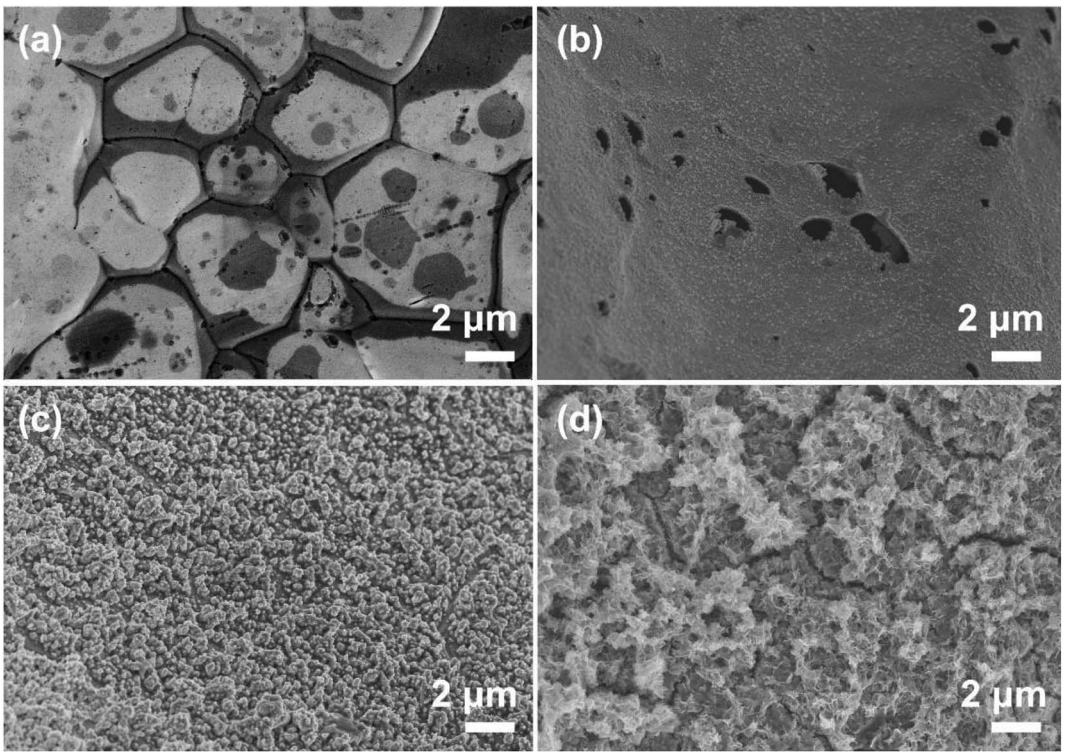

Fig. 4 The SEM images of (a) Ni, (b) Pd(CD)/Ni, (c) Pd(CPD)/Ni and (d) Pd-Co_3O_4/Ni foams.

in Fig. 5(b–d), PA was the main product. Only a small amount of 2-CPA was generated, and 4-CPA was undetectable by HPLC. The rate of dechlorination of 2-CPA was slower than that of 4-CPA, since the attached –OCH_2COOH group hindered cleavage of the C–Cl bond at the 2-position. The selectivity of the dechlorination was similar to that reported in the literature,[38,55] in which electrocatalytic dechlorination of 2,4-D first yielded the mono-chlorinated intermediates, 2-CPA or 4-CPA, which were subsequently converted to PA, the ultimate dechlorinated product. The sum concentration of all products and the remaining reactants translated to about 95.9–101.0% of the initial total carbon mass, suggesting that the adsorption of these pollutants on the electrode was negligible during the reaction. The finding that the total amount of carbon was unchanged is consistent with results reported in the literature.[40,57]

Fig. 5(e) shows the variation of CEs on Pd-Co_3O_4/Ni, Pd(CPD)/Ni and Pd(CD)/Ni foam electrodes over time at a current density of 1.5 mA cm^{-2}. All of the CEs increased first and then declined as the reaction time was extended. This is likely due to establishment of an equilibrium between the hydrogen atoms in the solid solution phase and those in the metal hydride phase in the preliminary stage.[57] Subsequently, the H^*_{ads} in solid solution is consumed for dechlorination of 2,4-D. Consequently, an initial rise of the CE was observed. The subsequent reduction of CE might be due to limited mass transfer of the reactants.[11,58]

The maximal CEs of the Pd-Co_3O_4/Ni, Pd(CPD)/Ni and Pd(CD)/Ni foam electrodes at a current density of 1.5 mA cm^{-2} were determined to be 12.1%, 4.8% and 3.7%, respectively. Clearly, the maximum CE of the Pd-Co_3O_4/Ni foam electrode was ~2.5-fold that of the Pd(CPD)/Ni electrode and ~3.3-fold that of the Pd(CD)/Ni electrode. Therefore, the Pd-Co_3O_4/Ni foam electrode has superior dechlorination activity compared with the Pd(CPD)/Ni and Pd(CD)/Ni foam electrodes.

Regarding the electrochemical dechlorinated process, two mechanisms that have been proposed involve direct electron transfer and indirect reduction *via* atomic H*.[59–61] As shown in Fig. 5(a) where no Pd catalyst was used, the Ni and Co_3O_4/Ni foams exhibited almost no decrease of 2,4-D at a current density of 1.5 mA cm^{-2} over 120 min of electrolysis, suggesting an indirect electrochemical dechlorination process in the reaction of 2,4-D.[62] In this work, the indirect reduction mechanism may involve the following pathways,[63] as shown in eqn (2)–(5):

$$2H_2O + M + 2e^- \rightarrow 2\left(H^*_{ads}\right)M + 2OH^- \quad (2)$$

$$R\text{–}Cl + AS \leftrightarrow (R\text{–}Cl)_{ads}AS \quad (3)$$

$$(R - Cl)_{ads}AS + e^- + \left(H^*_{ads}\right)M \rightarrow (R - H)_{ads}AS + Cl^- + M \quad (4)$$

$$(R\text{–}H)_{ads}AS \leftrightarrow R\text{–}H + AS \quad (5)$$

where AS is the active sites for reactant adsorption, H^*_{ads} is adsorbed atomic hydrogen, and M is the Pd catalyst.

3.3. Enhanced mechanism

It was reasonable to speculate that the introduction of Co_3O_4 could accelerate the hydrogen evolution reaction. To confirm this hypothesis, LSV measurements of Ni, Pd(CPD)/Ni, Pd-

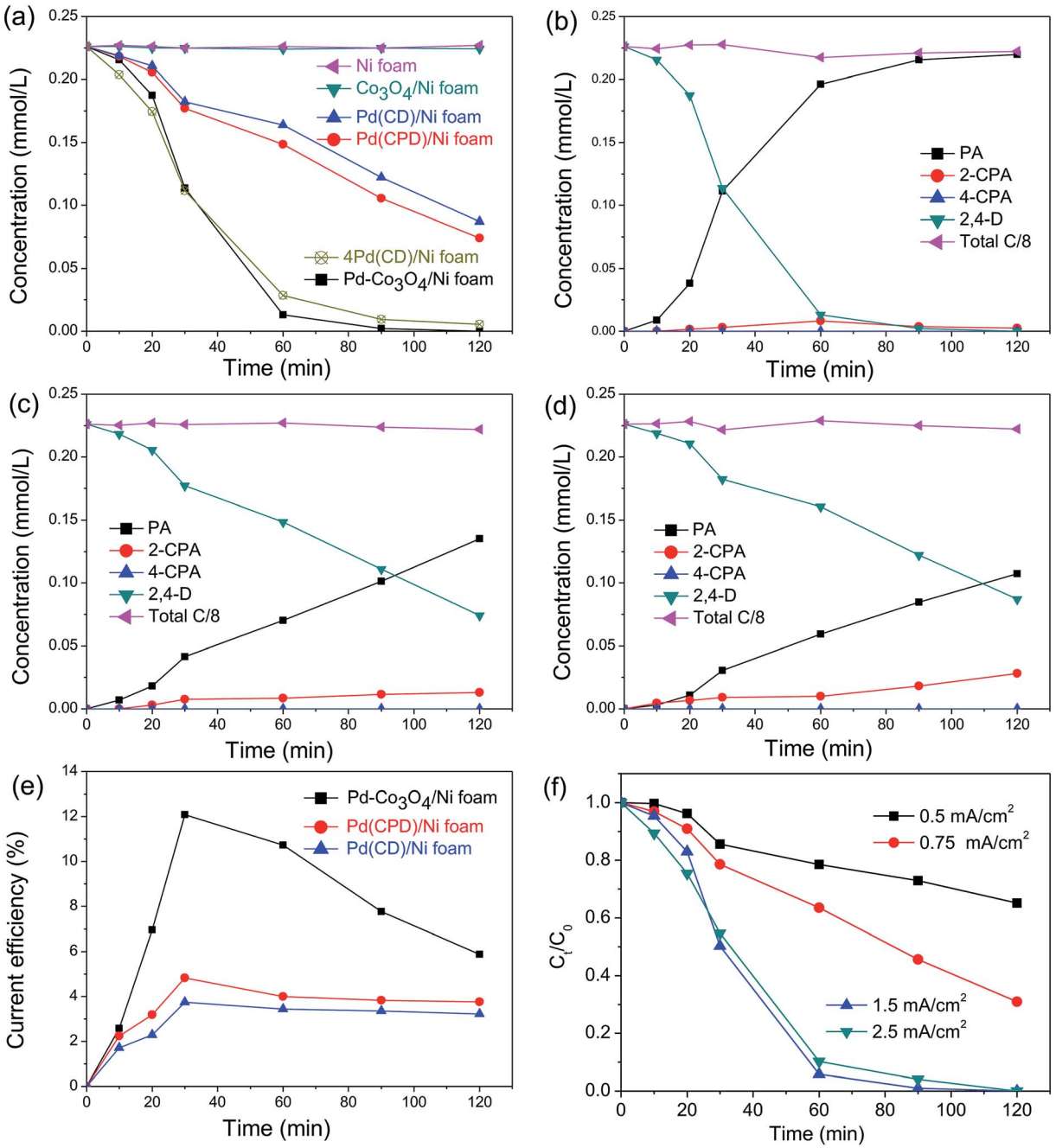

Fig. 5 (a) The time course of 2,4-D concentration with as-prepared electrodes of Ni, Co_3O_4/Ni, Pd(CD)/Ni, Pd(CPD)/Ni, 4Pd(CD)/Ni and Pd-Co_3O_4/Ni foams; the time course of PA, 2-CPA, 4-CPA and 2,4-D concentrations with the (b) Pd-Co_3O_4/Ni foam electrode, (c) Pd(CPD)/Ni foam electrode and (d) Pd(CD)/Ni foam electrode; (e) the current efficiencies as functions of dechlorination time on Pd-Co_3O_4/Ni, Pd(CPD)/Ni and Pd(CD)/Ni foam electrodes at a current density of 1.5 mA cm^{-2}; (f) the dechlorination efficiencies as functions of time on the Pd-Co_3O_4/Ni foam electrode at current densities of 0.5, 0.75, 1.5 and 2.5 mA cm^{-2}.

Co_3O_4/Ni, and Co_3O_4/Ni foams were recorded in the catholyte in the absence of 2,4-D. As shown in Fig. 6(a), the rates of HER were in the following order: Ni foam < Co_3O_4/Ni foam < Pd(CPD)/Ni foam < Pd-Co_3O_4/Ni foam. The introduction of Co_3O_4 on the Ni foam resulted in an improvement of potential of hydrogen evolution from −1.0 V (bare Ni foam) to −0.9 V (Co_3O_4/Ni foam). However, the Co_3O_4/Ni foam electrode does not enable dechlorination because Pd is the key catalyst to store atomic H*, which is the major reductant for catalytic hydrodechlorination.[40,56,59] The potential of Pd-Co_3O_4/Ni foam (−0.50 V) was relatively positive compared to that of Pd(CPD)/Ni foam (−0.6 V), further indicating that HER was promoted in the presence of Co_3O_4. Although it would be inappropriate to draw conclusions on the effectiveness of dechlorination based simply on the LSV data for the HER as a side reaction in the dechlorination of 2,4-D, it could offer some insights into the process.

Generation of adsorbed atomic H^*_{ads} was confirmed on the Pd-Co_3O_4/Ni foam electrode by the CV curves shown in

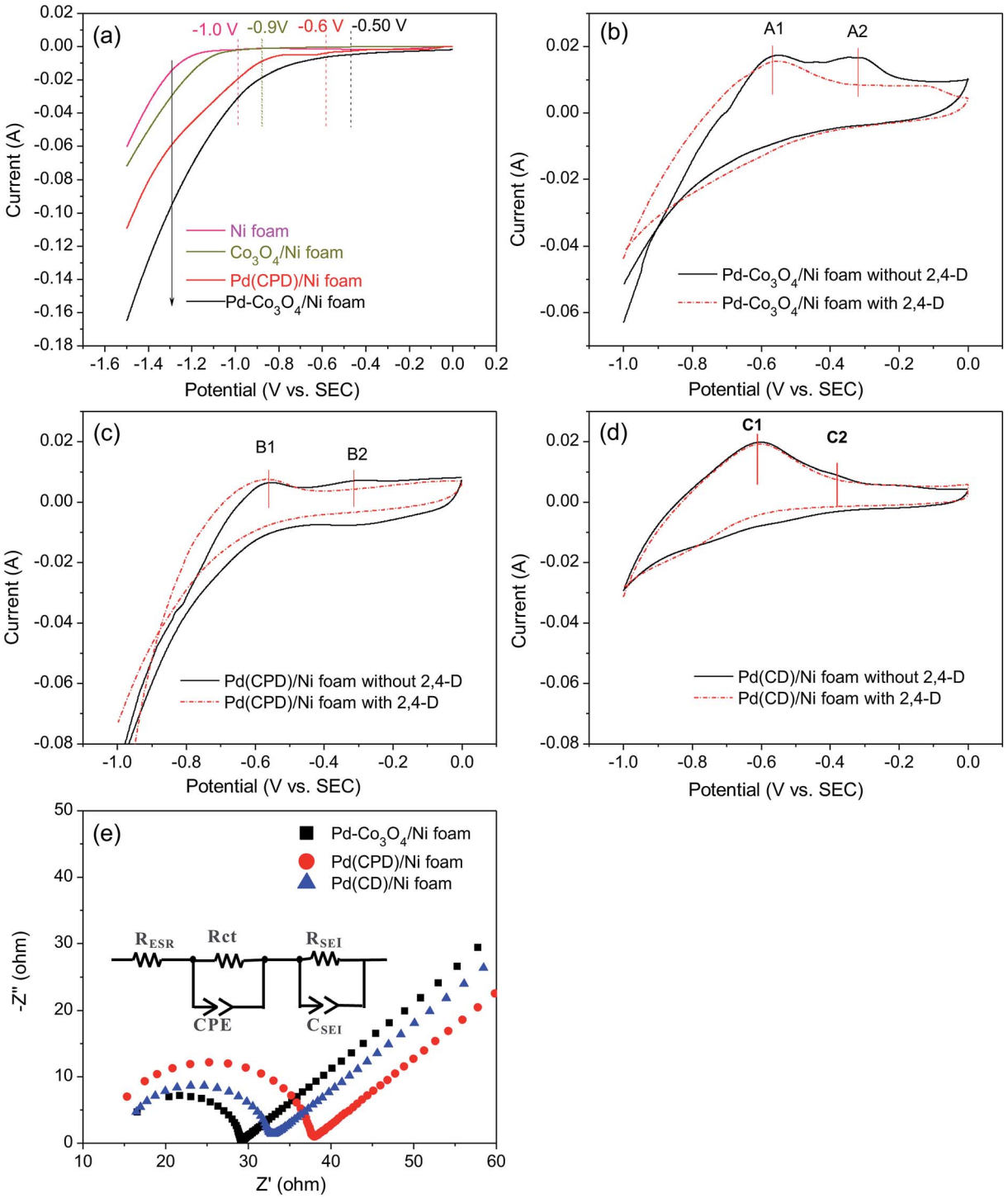

Fig. 6 (a) LSV of Pd-Co_3O_4/Ni, Pd(CPD)/Ni, Co_3O_4/Ni and Ni foams; (b) CV of Pd-Co_3O_4/Ni foam; (c) CV of Pd(CPD)/Ni foam; (d) CV of Pd(CD)/Ni foam; (e) Nyquist diagrams of Pd-Co_3O_4/Ni, Pd(CPD)/Ni and Pd(CD)/Ni foams. The inset is the equivalent electrical circuit used to fit the EIS data (R_{ESR} is the electrolyte resistance, R_{ct} denotes the charge transfer resistance, CPE represents the constant phase-angle element, R_{SEI} and C_{SEI} are the pseudo capacitance and resistance of the solid/electrolyte interface, respectively). Experimental conditions: 2,4-D concentration = 50 mg L^{-1} and support electrolyte (Na_2SO_4) concentration = 0.017 mol L^{-1}.

Fig. 6(b–d). Adsorbed atomic H^*_{ads} oxidation peaks were observed within potential ranges of −0.60 to −0.50 V and −0.40 to −0.30 V without addition of 2,4-D. According to previous studies,[16,64] the two oxidation peaks could be associated with desorption of atomic H^*_{ads} adsorbed on {111} and {100} planes of polycrystalline Pd. Since the adsorption energy of hydrogen on Pd {111} facets is stronger than that on {100} facets, the oxidation peak at 1-site (more negative potential) and 2-site (more positive potential) should be assigned to the H^*_{ads} desorption on {111} and {100} planes of Pd. Interestingly, upon addition of 2,4-

D, the peaks at A2, B2 and C2 totally disappeared, while peaks at A1, B1 and C1 were mostly unchanged. It can be concluded that active adsorbed atomic H^*_{ads} located at {111} planes were the key active hydrogen species for dechlorination. Furthermore, the current density of the A2 peak (4.2 mA cm^{-2}) was higher than those of the B2 peak (1.93 mA cm^{-2}) and C2 peak (1.83 mA cm^{-2}), suggesting that more active adsorbed atomic H^*_{ads} was present on the Pd-Co_3O_4/Ni foam.

In addition, on the basis of the results and according to the literature,[37] it was speculated that Co_3O_4 in the hybrid materials may have set up a hierarchical multi-porous structure,[53,65] which can facilitate charge- and mass-transfer processes. To confirm this hypothesis, EIS analyses of the Pd-Co_3O_4/Ni foam, Pd(CPD)/Ni foam and Pd(CD)/Ni foam electrodes were conducted. In Fig. 6(e), the EIS curves show an equivalent series resistance R_{ESR} in the high frequency region, one depressed arc radius corresponding to the electron transfer resistance (R_{ct}), a double layer capacitor represents the constant phase-angle element (CPE) region and an inclined spike reveals an electrode/electrolyte interface effect in the low frequency region.[10,63,66] The size of the arc radius was reduced, revealing that the presence of Co_3O_4 decreased the interface impedance and accelerated electron transfer. The arc radius of the Pd(CD)/Ni foam was smaller than that of the Pd(CPD)/Ni foam, which can be explained by the resistivity of the conductive material being substantially increased as the Pd particle size decreased, as shown in other studies.[67,68]

In summary, the Pd-Co_3O_4/Ni foam enhances dechlorination because of the key role played by Co_3O_4, which accelerates the dissociation of H_2O and electron transfer. This then produces more atomic H* intermediates, and more atomic H* is adsorbed by the Pd catalyst to facilitate dechlorination. Hence, the presence of Co_3O_4 greatly enhances dechlorination activity.

3.4. Reusability of the Pd-Co_3O_4/Ni foam electrode

Electrode stability is always a crucial concern for the practical application of contaminant degradation. The Pd-Co_3O_4/Ni foam electrode was evaluated to verify electrode stability *via* five cycles of 2,4-D dechlorination at a current density of 1.5 mA cm^{-2} as shown in Fig. 7. The 2,4-D removal efficiencies were 94.2%, 93.9%, 93.7%, 93.5%, and 93.2% after 60 min in each cycle, respectively. The 2,4-D removal efficiency was 100% after 120 min in each cycle. There was no significant change in the 2,4-D removal efficiency after five reaction cycles, which indicated that the Pd-Co_3O_4/Ni foam had good reusability. Furthermore, it was found that about 1.09% Pd was lost, as analyzed by ICP-OES during the dechlorination of 2,4-D using the Pd-Co_3O_4/Ni foam electrode over five reaction cycles, indicating that the electrode was stable.

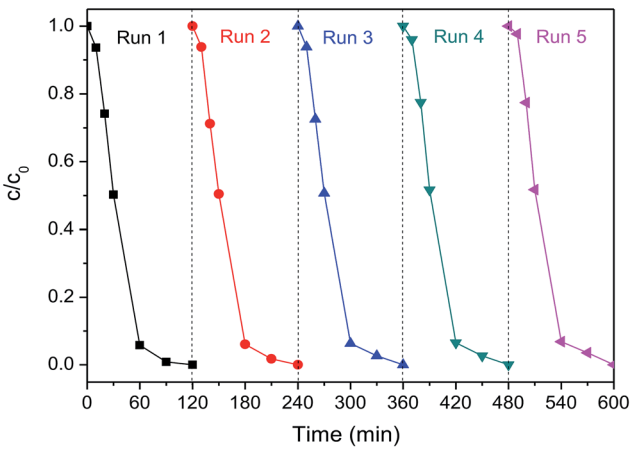

Fig. 7 The 2,4-D removal efficiency by dechlorination using the Pd-Co_3O_4/Ni foam for five cycles at a current density of 1.5 mA cm^{-2}.

4. Conclusions

A well-designed Pd-Co_3O_4/Ni foam with high catalytic activity and excellent long-term durability for electrochemical dechlorination of 2,4-D was produced by a facile and cost-effective two-step synthesis. The Pd-Co_3O_4/Ni foam exhibited higher dechlorination efficiency and CE than Pd(CPD)/Ni and Pd(CD)/Ni foam electrodes. After 60 min of reaction, 94.2% of 2,4-D was dechlorinated with a maximum CE of 12.1%. The Co_3O_4 layer with hierarchical multi-porous structures covering the surface of the Ni foam promoted the production of atomic H* and accelerated charge- and mass-transfer. This provided the Pd catalyst with more active adsorbed atomic H^*_{ads}, which has been proven to play a dominant role in dechlorination of 2,4-D.

Conflicts of interest

There are no conflicts to declare.

Acknowledgements

This work was supported by the National Natural Science Foundation of China (Grant 21477117) and the Zhejiang Provincial Natural Science Foundation of China (Grants LZ18B070001, LGF18E080017 and LR14E080001).

References

1 Y. Xi, M. Mallavarapu and R. Naidu, *Appl. Clay Sci.*, 2010, **49**, 255–261.
2 N. Maleki, A. Safavi and H. R. Shahbaazi, *Anal. Chim. Acta*, 2005, **530**, 69–74.
3 R. A. Rebich, R. H. Coupe and E. M. Thurman, *Sci. Total Environ.*, 2004, **321**, 189–199.
4 J. R. de Lipthay, S. R. Sorensen and J. Aamand, *Environ. Pollut.*, 2007, **148**, 83–93.
5 K. Shareef and G. Shaw, *Chemosphere*, 2008, **72**, 8–15.
6 S. Cenkci, M. Yildiz, I. H. Cigerci, A. Bozdag, H. Terzi and E. S. A. Terzi, *Ecotoxicol. Environ. Saf.*, 2010, **73**, 1558–1564.
7 B. Bukowska and K. Hutnik, *Pestic. Biochem. Physiol.*, 2006, **85**, 174–180.
8 B. Yang, S. Wang, G. Yu and Y. Zhou, *Sep. Purif. Technol.*, 2008, **63**, 353–359.
9 Z. Q. He, L. Y. Zhan, Q. Wang, S. Song, J. M. Chen, K. R. Zhu, X. H. Xu and W. P. Liu, *Sep. Purif. Technol.*, 2011, **80**, 526–532.
10 R. Mao, N. Li, H. C. Lan, X. Zhao, H. J. Liu, J. H. Qu and M. Sun, *Environ. Sci. Technol.*, 2016, **50**, 3829–3837.

11 Y. H. Xu, Q. Q. Cai, H. X. Ma, Y. He, H. Zhang and C. A. Ma, *Electrochim. Acta*, 2013, **96**, 90–96.
12 H. Zilouei, B. Guieysse and B. Mattiasson, *Process Biochem.*, 2006, **41**, 1083–1089.
13 S. Eker and F. Kargi, *J. Hazard. Mater.*, 2006, **135**, 365–371.
14 H. Shimakoshi, M. Tokunaga, T. Baba and Y. Hisaeda, *Chem. Commun.*, 2004, 1806–1807, DOI: 10.1039/b406400c.
15 M. Ratti, S. Canonica, K. McNeill, J. Bolotin and T. B. Hofstetter, *Environ. Sci. Technol.*, 2015, **49**, 9797–9806.
16 G. M. Jiang, M. N. Lan, Z. Y. Zhang, X. S. Lv, Z. M. Lou, X. H. Xu, F. Dong and S. Zhang, *Environ. Sci. Technol.*, 2017, **51**, 7599–7605.
17 R. Mao, H. C. Lan, L. Yan, X. Zhao, H. J. Liu and J. H. Qu, *Environ. Sci.: Nano*, 2018, **5**, 2282–2292.
18 J. S. Zhou, Z. M. Lou, J. Xu, X. X. Zhou, K. L. Yang, X. Y. Gao, Y. L. Zhang and X. H. Xu, *Chem. Eng. J.*, 2019, **358**, 1176–1185.
19 B. B. Huang, A. A. Isse, C. Durante, C. H. Wei and A. Gennaro, *Electrochim. Acta*, 2012, **70**, 50–61.
20 Q. Shi, H. Wang, S. L. Liu and Z. Y. Bian, *RSC Adv.*, 2014, **4**, 56263–56272.
21 J. S. Zhou, Z. M. Lou, K. L. Yang, J. Xu, Y. Z. Li, Y. L. Liu, S. A. Baig and X. H. Xu, *Appl. Catal., B*, 2019, **244**, 215–224.
22 B. P. Chaplin, M. Reinhard, W. F. Schneider, C. Schuth, J. R. Shapley, T. J. Strathmann and C. J. Werth, *Environ. Sci. Technol.*, 2012, **46**, 3655–3670.
23 I. F. Cheng, Q. Fernando and N. Korte, *Environ. Sci. Technol.*, 1997, **31**, 2443.
24 Q. Qu, G.-L. Pan, Y.-T. Lin and C.-W. Xu, *Int. J. Hydrogen Energy*, 2018, **43**, 14252–14264.
25 C. X. Zhao, H. Luo, F. Chen, P. Zhang, L. H. Yi and K. Y. You, *Energy Environ. Sci.*, 2014, **7**, 1700–1707.
26 Z. Q. He, J. J. Sun, J. Wei, Q. Wang, C. X. Huang, J. M. Chen and S. Song, *J. Hazard. Mater.*, 2013, **250**, 181–189.
27 H. Husin, W.-N. Su, C.-J. Pan, J.-Y. Liu, J. Rick, S.-C. Yang, W.-T. Chuang, H.-S. Sheu and B.-J. Hwang, *Int. J. Hydrogen Energy*, 2013, **38**, 13529–13540.
28 F. Li, H. Huang, G. Li and D. Y. C. Leung, *J. Nanopart. Res.*, 2019, 21.
29 L. Han, S. Dong and E. Wang, *Adv. Mater.*, 2016, **28**, 9266–9291.
30 J. H. Wang, W. Cui, Q. Liu, Z. C. Xing, A. M. Asiri and X. P. Sun, *Adv. Mater.*, 2016, **28**, 215–230.
31 G. Yanalak, A. Aljabour, E. Aslan, F. Ozel, I. H. Patir, M. Kus and M. Ersoz, *Electrochim. Acta*, 2018, **291**, 311–318.
32 L. J. Zhang, Y. Y. Zhang, S. L. Huang, Y. L. Yuan, H. Li, Z. Y. Jin, J. H. Wu, Q. F. Liao, L. Hu, J. G. Lu, S. C. Ruan and Y. J. Zeng, *Electrochim. Acta*, 2018, **281**, 189–197.
33 E. Skulason, V. Tripkovic, M. E. Bjoerketun, S. Gudmundsdottir, G. Karlberg, J. Rossmeisl, T. Bligaard, H. Jonsson and J. K. Norskov, *J. Phys. Chem. C*, 2010, **114**, 22374.
34 X. Sun, J. Huo, Y. D. Yang, L. Xu and S. Y. Wang, *J. Energy Chem.*, 2017, **26**, 1136–1139.
35 J. Lee, W. Shim, J. S. Noh and W. Lee, *ChemPhysChem*, 2012, **13**, 1395–1403.
36 J. L. Lado, X. Wang, E. Paz, E. Carbo-Argibay, N. Guldris, C. Rodriguez-Abreu, L. Liu, K. Kovnir and Y. V. Kolen'ko, *ACS Catal.*, 2015, **5**, 6503–6508.
37 C. Yuan, L. Yang, L. Hou, L. Shen, X. Zhang and X. W. Lou, *Energy Environ. Sci.*, 2012, **5**, 7883–7887.
38 J. J. Li, H. L. Liu, X. W. Cheng, Q. H. Chen, Y. J. Xin, Z. P. Ma, W. X. Xu, J. Ma and N. Q. Ren, *Chem. Eng. J.*, 2013, **225**, 489–498.
39 Y. Zhang, J. H. Li, J. Bai, Z. X. Shen, L. S. Li, L. G. Xia, S. Chen and B. X. Zhou, *Environ. Sci. Technol.*, 2018, **52**, 1413–1420.
40 K. R. Zhu, S. A. Baig, J. Xu, T. T. Sheng and X. H. Xu, *Electrochim. Acta*, 2012, **69**, 389–396.
41 L. Tang, S. Zhang, G. M. Zeng, Y. Zhang, G. D. Yang, J. Chen, J. J. Wang, J. J. Wang, Y. Y. Zhou and Y. C. Deng, *J. Colloid Interface Sci.*, 2015, **445**, 1–8.
42 J. J. Li, H. L. Liu, X. W. Cheng, Y. J. Xin, W. X. Xu, Z. P. Ma, J. Ma, N. Q. Ren and Q. Li, *Ind. Eng. Chem. Res.*, 2012, **51**, 15557–15563.
43 J. J. Li, C. Luan, Y. Q. Cui, H. X. Zhang, L. Wang, H. Wang, Z. H. Zhang, B. Zhao, H. W. Zhang, X. Y. Zhang and X. W. Cheng, *Sep. Purif. Technol.*, 2019, **211**, 198–206.
44 S. Pocovi-Martinez, I. Zumeta-Dube and D. Diaz, *J. Nanomater.*, 2019, **2019**, 6461493.
45 S. L. Xiong, C. Z. Yuan, M. F. Zhang, B. J. Xi and Y. T. Qian, *Chem.–Eur. J.*, 2009, **15**, 5320–5326.
46 G. Yanalak, A. Aijabour, E. Aslan, F. Ozel and I. H. Patir, *Int. J. Hydrogen Energy*, 2018, **43**, 17185–17194.
47 G. B. Hoflund and Z. H. Li, *Appl. Surf. Sci.*, 2006, **253**, 2830–2834.
48 J. Y. Luo, M. Meng, X. Li, X. G. Li, Y. Q. Zha, T. D. Hu, Y. N. Xie and J. Zhang, *J. Catal.*, 2008, **254**, 310–324.
49 X. D. Zhang, J. L. Xiao, X. Y. Zhang, Y. Meng and D. Xiao, *Electrochim. Acta*, 2016, **191**, 758–766.
50 Z. Q. Liu, K. Xiao, Q. Z. Xu, N. Li, Y. Z. Su, H. J. Wang and S. Chen, *RSC Adv.*, 2013, **3**, 4372–4380.
51 Z. Q. Liu, Q. Z. Xu, J. Y. Wang, N. Li, S. H. Guo, Y. Z. Su, H. J. Wang, J. H. Zhang and S. Chen, *Int. J. Hydrogen Energy*, 2013, **38**, 6657–6662.
52 J. A. Mwanda and A. Cuesta, *Electrochim. Acta*, 2018, **292**, 419–424.
53 B. Liu, J. Cheng, H.-Q. Peng, D. Chen, X. Cui, D. Shen, K. Zhang, T. Jiao, M. Li, C.-S. Lee and W. Zhang, *J. Mater. Chem. A*, 2019, **7**, 775–782.
54 Q. M. Sun, N. Wang, Q. M. Bing, R. Si, J. Y. Liu, R. S. Bai, P. Zhang, M. J. Jia and J. H. Yu, *Chem*, 2017, **3**, 477–493.
55 Z. R. Sun, G. Song, R. Du and X. Hu, *RSC Adv.*, 2017, **7**, 22054–22062.
56 C. Sun, Z. M. Lou, Y. Liu, R. Q. Fu, X. X. Zhou, Z. Zhang, S. A. Baig and X. H. Xu, *Chem. Eng. J.*, 2015, **281**, 183–191.
57 C. Sun, S. A. Baig, Z. M. Lou, J. Zhu, Z. X. Wang, X. Li, J. H. Wu, Y. F. Zhang and X. H. Xu, *Appl. Catal., B*, 2014, **158**, 38–47.
58 A. I. Tsyganok and K. Otsuka, *Appl. Catal., B*, 1999, **22**, 15–26.
59 W. J. Xie, S. H. Yuan, X. H. Mao, W. Hu, P. Liao, M. Tong and A. N. Alshaulabkeh, *Water Res.*, 2013, **47**, 3573–3582.
60 A. Z. Li, X. Zhao, Y. N. Hou, H. J. Liu, L. Y. Wu and J. H. Qu, *Appl. Catal., B*, 2012, **111**, 628–635.

61 T. Li and J. Farrell, *Environ. Sci. Technol.*, 2000, **34**, 173–179.
62 Z. Q. He, Q. W. Jian, J. T. Tang, T. Xu, J. L. Xu, Z. S. Yu, J. M. Chen and S. Song, *Electrochim. Acta*, 2016, **222**, 488–498.
63 Z. Q. He, Y. W. Tong, S. L. Ni, X. C. Ye, C. P. Makwarimba, X. W. Huang, S. H. Zhang and S. Song, *Electrochim. Acta*, 2018, **292**, 685–696.
64 Z. M. Lou, J. S. Zhou, M. Sun, J. Xu, K. L. Yang, D. Lv, Y. P. Zhao and X. H. Xu, *Chem. Eng. J.*, 2018, **352**, 549–557.
65 L. Yang, H. Zhou, X. Qin, X. Guo, G. Cui, A. M. Asiri and X. Sun, *Chem. Commun.*, 2018, **54**, 2150–2153.
66 J. Yesuraj, S. A. Suthanthiraraj and O. Padmaraj, *Mater. Sci. Semicond. Process.*, 2019, **90**, 225–235.
67 R. Mahesh, R. Mahendiran, A. K. Raychaudhuri and C. N. R. Rao, *Appl. Phys. Lett.*, 1996, **68**, 2291–2293.
68 T. H. Tsai, S. C. Chiou and S. M. Chen, *Int. J. Electrochem. Sci.*, 2011, **6**, 3333–3343.